Bulletin of the Seismological Society of America, Vol. 104, No. 6, pp. 2809–2826, December 2014, doi: 10.1785/0120140097

Assessment of Site Effects in Alpine Regions through Systematic Site Characterization of Seismic Stations

by Clotaire Michel, Benjamin Edwards, Valerio Poggi, Jan Burjánek, Daniel Roten, Carlo Cauzzi, and Donat Fäh

Abstract In the framework of the renewal project of the Swiss Strong Motion Network (SSMNet), a procedure for site characterization has been established. The aim of the procedure was to systematically derive realistic 1D velocity profiles at each station. It is mainly based on the analysis of surface waves, particularly from passive experiments, and includes cross checks of the derived amplification functions with those obtained through spectral modeling of recorded earthquakes. The systematic use of three component surface-wave analysis, allowing the derivation of both Rayleigh and Love dispersion curves, also contributes to the improvement of the quality of the retrieved profiles.

The procedure is applied to the 30 SSMNet stations installed on various site types within the project, covering different aspects of seismic risk. The characterization of these 30 sites gives an overview of the variety of possible effects of surface geology on ground motion in the Alpine area. Such effects ranged from deamplification at hard-rock sites to amplification up to a factor of 15 in lacustrine sediments with respect to the Swiss reference rock velocity model. The derived velocity profiles are shown to reproduce observed amplification functions from empirical spectral modeling. Although many sites are found to exhibit 1D behavior, the procedure allows the detection and qualification of 2D and 3D effects. The sites are therefore classified with respect to the occurrence of 2D/3D resonance and edge-generated surface waves. In addition to the large and deeply incised alpine valleys of the Rhône, the Rhine, and the Aar, smaller structures such as local alpine valleys and alluvial fans are shown to exhibit 2D/3D behavior.

Introduction

Local site conditions have a significant impact on earthquake ground motions. This so-called site effect is dominantly controlled by variations in the shear-wave velocity of the subsurface. For instance, interfaces between high *S*-wave velocities in bedrock and low velocities in sediments can lead to the development of strong amplification and resonance phenomena. Urban areas around the world are often built on sedimentary basins to ease the access to water and avoid steep topography. Site effects therefore constitute a large part of the seismic hazard in urban areas (e.g., in Mexico City [Bard *et al.*, 1988], Caracas [Duval *et al.*, 2001], Los Angeles [Wald and Graves, 1998], Tokyo [Yamanaka *et al.*, 1989], or Bangkok [Poovarodom and Plalinyot, 2013]).

Assessment of amplification phenomena related to a site is often performed with an assumption of horizontally layered media (1D structure) using the theoretical *SH*-wave transfer function (Knopoff, 1964). However, non-1D effects related to sedimentary basins have been discussed since the 1970s and observed in strong-motion recordings (e.g., King and Tucker, 1984). For instance, Thompson *et al.* (2009, 2012) evaluated and classified the limitations of the 1D assumption. The significant variability of observed amplification has also justified numerous numerical studies.

To fully consider the expected amplification at a site located in a narrow sedimentary basin, 3D effects should clearly be considered. However, although computing capabilities are improving dramatically, 3D numerical simulation of large areas still has a high computational cost. Furthermore, a good knowledge of the structure is required, which also defines the useful frequency band for modeling. Consequently, 3D models are typically developed at sites that have been previously well studied. In Switzerland, for instance, 2D effects in the Rhône valley have been quantified by extensive studies combining direct observations and modeling (Steimen *et al.*, 2003; Roten *et al.*, 2006, 2008; Ermert *et al.*, 2014). Before being able to model 2D/3D effects, however, local assessment of 1D velocity profiles is always needed, along with their lateral variation. Moreover, Burjánek *et al.* (2014) analyzed

25 sites with pronounced topography and showed that observed amplifications at such sites are tightly linked with the local subsurface structure rather than terrain geometry.

Explaining recorded ground motion through deconvolution of source, propagation, and site effects is a primary goal of engineering seismology. High quality characterization through independent geophysical investigation of each instrumented site is necessary to properly isolate and explain site effects and ultimately refine estimation of earthquake magnitude and seismic attenuation. The aim of this article is therefore to propose a procedure able to provide high quality but affordable site characterization for seismic stations including validation. The procedure quantifies site effects and qualitatively identifies 2D/3D effects.

The proposed method is implemented within the framework of the renewal project of the Swiss Strong Motion Network (SSMNet). The procedure for characterization of the sites of 30 newly installed stations is applied systematically. Geophysical site investigations are based on three-component (3C) surface-wave analysis, particularly of ambient vibration array recordings (Fäh *et al.*, 2008; Poggi and Fäh, 2010). A new procedure based on spectral modeling of earthquake ground motion at these stations (Edwards *et al.*, 2013) has been used to check the validity of the site characterization. Moreover, the whole process checks for 2D/3D effects, due to edge-generated surface waves (EGSW) and 2D/3D resonances. Sites are classified and compared with the classification proposed by Bard and Bouchon (1985) for 2D resonance in sedimentary basins.

2D/3D Phenomena

Bard and Bouchon (1980, 1985) identified two non-1D phenomena in sediment-filled valleys: (1) the inclined interfaces at the edge create laterally propagating surface waves that amplify the ground motion and (2) sufficiently slender valleys with large velocity contrasts exhibit 2D resonances or normal modes. Depending on the characteristics of the valley (velocity contrast and shape), one or both phenomena play a role in the transfer function (Bard and Bouchon, 1985). These authors also provide empirical limits of these characteristics for the occurrence of 2D resonance based on a numerical study.

Edge-generated surface waves were observed by Field (1996), Chavez-Garcia *et al.* (1999), Joyner (2000), Lebrun *et al.* (2001), Cornou and Bard (2003), and Roten *et al.* (2008). Moreover, numerical modeling has often been used in the literature to reproduce EGSW and wave-focusing effects (e.g., Paolucci and Morstabilini, 2006; Lenti *et al.*, 2009; Faccioli *et al.*, 2010). Kawase (1996) showed such effects were responsible for the large damage in Kobe 1995; the well-known "Kobe effect." EGSW can generally be recognized on time traces of earthquake recordings in basins as long duration surface-wave trains. They typically occur on a broad frequency range starting from the fundamental frequency of the valley (e.g., Cornou and Bard, 2003; Cauzzi *et al.*, 2011). The amplification function is then smooth and of large amplitude as found, for instance, by Lebrun *et al.* (2001) in Grenoble, France. Cornou and Bard (2003) proposed to compute the ratio of the observed amplification function to the 1D theoretical transfer function, termed the aggravation factor, to characterize these EGSW.

The 2D/3D normal modes are characterized by a constant resonance frequency on the entire valley, at which the motion is in phase and exhibits a shape characteristic of the considered mode (Roten *et al.*, 2006). 2D resonance was particularly observed in the Rhône valley in Switzerland (Steimen *et al.*, 2003; Roten *et al.*, 2006; Ermert *et al.*, 2014; Poggi *et al.*, 2014). Several authors underlined the shift of fundamental frequency peak compared with 1D assumption in 2D/3D cases (e.g., Guéguen *et al.*, 2007; Le Roux *et al.*, 2012), and a deviation of the dispersion curves from the 1D case that needs to be taken into account in the inversion (Roten and Fäh, 2007). However, without a good knowledge of the basin geometry, highlighting eventual shifts between 1D modeling and observed peaks is not possible. Steimen *et al.* (2003) and Roten *et al.* (2006) recommend the use of the reference station method to detect 2D modal shapes. Further, Ermert *et al.* (2014) and Poggi *et al.* (2014) proposed to apply modal analysis approaches from mechanical and civil engineering to determine the resonance frequencies and modal shapes of the basin. Alternatively, Fritsche *et al.* (2005) proposed to use the polarization of waves at the resonance frequency using azimuthal horizontal-to-vertical (H/V) spectral ratios. A strong polarization in the valley axis is an indication for the *SH*-mode shape and, therefore, the occurrence of 2D resonance. Ermert *et al.* (2014) followed the same approach but, instead of the azimuthal H/V, used the method developed by Burjánek *et al.* (2010) to characterize the polarization and showed the equivalence with the modal analysis approach.

SSMNet Renewal Project

The SSMNet is currently undergoing major upgrades (Clinton *et al.*, 2011). In the framework of this renewal project, 30 state-of-the-art strong-motion stations in free-field conditions have been installed during a first phase (2009–2013), and an additional 70 stations are planned in a second phase (2013–2019). The current status of the SSMNet is displayed in Figure 1. The selection of instrumented sites, eventually replacing existing strong-motion dial-up stations, was made considering different aspects of seismic risk. This project achieved a better general spatial coverage over the country, while focusing on the instrumentation of areas with known historical earthquakes, on urban areas concentrating the largest risk exposure, and on areas with significant site amplification expected. As a result, the SSMNet stations widely sample typical sites of the alpine environment. Such sites are characterized by the presence of loose alluvium-filled valleys, alluvial fans, and steep slopes: often associated with significantly increased ground-motion amplitudes and therefore expected earthquake damage.

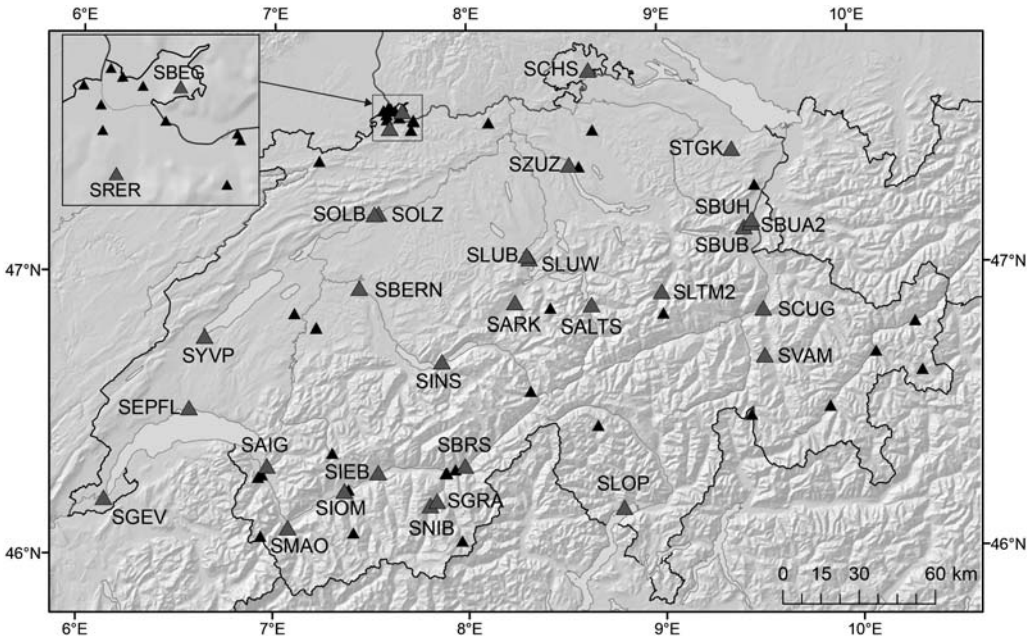

Figure 1. Modern stations of the Swiss Strong Motion Network at the end of phase 1 of the renewal project (triangles). Stations installed within the renewal project are displayed with larger gray symbols and their corresponding station code.

The self-noise of high-quality modern accelerometric stations (constituted e.g., by a broadband force-balance accelerometer writing on a 24-bit datalogger) is low enough and their dynamic range high enough to record with high fidelity both weak and strong ground motions (Cauzzi and Clinton, 2013). However, to take full advantage of this technology, disturbances from anthropogenic activities (traffic, industries, etc.) should be minimized at the installation sites. Therefore, new stations were not installed in electrical substations (transformer houses), which comprised the majority of sites in the old dial-up network, and the vicinity of train lines and roads was avoided if possible. Rigorous site testing was made for each site to estimate noise levels. One week of ambient vibrations were typically recorded and analyzed using the method of McNamara and Buland (2004) and compared with the accelerometric high and low noise models proposed by Cauzzi and Clinton (2013). The data collected during the project show that in many urban areas, strong local site amplification can result in noise levels that are above the high noise model. However, because the installation of stations on these urban sediments is a goal of the project, such high noise values must be accepted in particular cases. Nevertheless, diurnal variation and sharp peaks produced by local anthropogenic noise sources could be minimized.

A new design for station housing (Fig. 2) was developed within the project to ensure free-field conditions. Two different concrete vaults are used, a large one capable of hosting the whole seismic station and a smaller one hosting only the sensor with the electronics being installed in a cabinet in a nearby building. The vaults are screwed onto a reinforced concrete foundation. The foundation width (about 1 m) is small enough to minimize kinematic soil–structure interaction effects on the recorded ground motions. The foundation is itself anchored in the ground using steel bars as proposed by Gorini *et al.* (2010) for the Italian network. This design minimizes the influence of nearby structures on the ground motion that can, however, not be totally excluded in urban areas (Ditommaso *et al.*, 2010).

The stations for the first phase of the project (30 stations) uniformly comprise a Kinemetrics EpiSensor ES-T force-balanced accelerometer and Nanometrics Taurus digitizer. They continuously stream data through ADSL or GSM lines to the Swiss Seismological Service, in which the continuous data are archived. Data are made available to users through a local ArcLink server and the European Integrated waveform Data Archive (EIDA) node of ETH Zurich (see Data and Resources). State-of-health monitoring is undertaken through monitoring of the continuous data streams and using the PQLX software (McNamara *et al.*, 2009).

Site Characterization Procedure

An important component of the installation of modern seismic stations is the characterization of the seismic response of the site. For instance, strong-motion waveforms cannot be properly interpreted without adequate knowledge of the main geophysical and geotechnical properties of the site where they have been recorded. Furthermore, when developing ground-motion prediction equations, the inclusion of amplification due to local site effects is critical. Such effects are typically represented either via soil or rock categories or as a continuous function of the average shear-wave velocity (V_S) of the subsurface layers.

Figure 2. Alternative housing of the stations installed within the SSMNet renewal project. Left: small vault containing the sensor only and hut hosting the cabinet with the digitizer and communication instruments (station SYVP). Right: large vault containing the whole station (station SEPFL). The color version of this figure is available only in the electronic edition.

Depending on the objective, different levels of site characterization are available. These levels comprise diverse procedures with increasing complexity, which can be nevertheless categorized as follows:

1. simplified geological and geotechnical classification (e.g., design code approach);
2. geophysical characterization using a single parameter (e.g., V_{S30}, f_0);
3. 1D profiling of the linear elastic and eventually inelastic parameters; and
4. full microzonation using advanced 2D/3D models and nonlinear response analysis.

Given the different accuracy of these approaches in estimating the ground response, the level of characterization between different networks in the world and even within the same network can be very heterogeneous. For instance, in Italy, Luzi *et al.* (2010) compiled all the available information for each station, from the fundamental frequency of the site to the profiling of the geophysical properties obtained from borehole logging and seismic experiments. Di Capua *et al.* (2011) proposed a classification for sites with limited information. In Japan, velocity profiles from borehole logging are available for every KiK-net station (Aoi *et al.*, 2004). In Taïwan, the sites of the whole network have been classified for a long time (Lee *et al.*, 2001). In Iran (Zaré *et al.*, 1999), Turkey (Sandıkkaya *et al.*, 2009), and Puerto Rico (Odum *et al.*, 2013), 1D *S*-wave velocity profiles are provided at a number of sites using mostly active seismic techniques. In the United States, single parameter characterization is typically based on the average travel-time velocity over the first 30 m (V_{S30}) obtained from measurements or inferred from surface geology (Yong *et al.*, 2013).

Soil class and single parameter characterization represent the easiest approach and are generally recommended when large areas have to be mapped. Different site classifications exist (e.g., EC8 design code [Eurocode 8, 2004], Building Seismic Safety Council [2004], etc.) and V_{S30} is nowadays the preferred parameter to define class boundaries. However, they do not provide good resolution and cannot explain the whole variety of local surface effects on the ground motion (even though important) such as the amplification induced by resonance. This gap therefore leads to strong limitations when using these data for scientific purposes. On the other hand, extended site-specific microzonation studies are generally too demanding where many sites are involved and useful only for detailed modeling of few selected sites.

For the renewal of the SSMNet, therefore, we tried to strike the right balance between invested resources and reliability of the site characterization results. This is achieved through the determination for each individual site of a set of 1D velocity profiles that are compatible with observed site response features.

To this aim, a standard methodology has been established (Fig. 3). Using different profiles allows us to map the uncertainty in the site response prediction. At some particular sites, information about nonlinear parameters is also provided, which is nevertheless not discussed in this article. Moreover, at some sites, insights about the complex 2D/3D geometry were derived by analyzing and mapping the variability of fundamental frequency of resonance over the neighboring area of the seismic station. Finally, a number of engineering parameters, such as V_{S30} and the quarter-wavelength velocity as a function of frequency or wavelength, can then be easily derived from the measured velocity profiles together with their uncertainties. Even though the engineering parameters will evolve with time due to new advances in research, the availability of 1D velocity profiles will give the possibility to progressively incorporate new information without reassessing the sites.

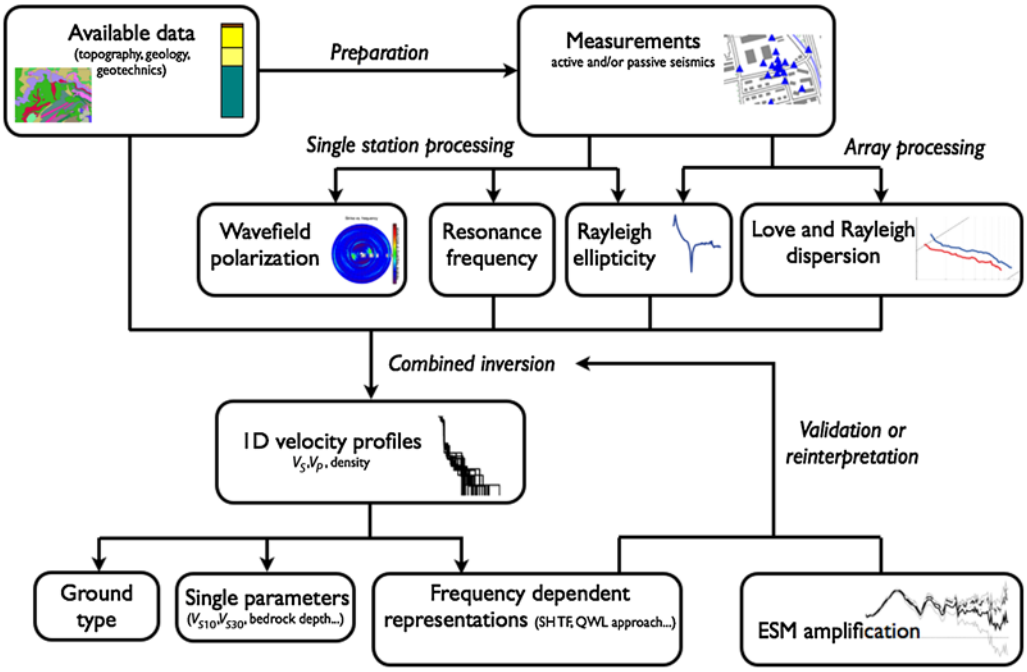

Figure 3. Site characterization procedure. The color version of this figure is available only in the electronic edition.

Retrieval of 1D Velocity Profiles

One-dimensional velocity profiles correspond to the sampling of the seismic velocities below the considered seismic station. Different methods exist to estimate 1D profiles. Borehole techniques such as sonic logging and downhole seismics are invasive but estimate the velocities with high resolution along the drilling line. Active and passive seismic surface-wave methods, on the other hand, are noninvasive but representative of finite volumes in the vicinity of the site. Small-scale heterogeneities within this volume are then averaged in a 1D profile, with resolution depending on the wavelengths involved in the method. This might lead to differences in the resulting 1D profiles with respect to direct borehole logging and between different methods.

The site characterization procedure adopted here is mainly based on surface-wave analysis of ambient vibration arrays. In some cases, it is complemented by surface-wave analysis of active seismic experiments (multichannel analysis of surface waves [MASW] technique). Passive techniques have been extensively applied and validated in the literature, especially in Europe (see Bard *et al.*, 2010, for a review). Combined passive and active surface-wave techniques have also been used to characterize strong-motion stations, for example, in Italy (Foti *et al.*, 2011) and Greece (Savvaidis *et al.*, 2006). Furthermore, part of the adopted procedure was already implemented to characterize 30 stations of the Swiss Seismic Networks (Havenith *et al.*, 2007; Fäh *et al.*, 2009).

A review of available geological, topographical, and geotechnical information is first performed to design geophysical experiments, to determine where the 1D assumption is valid, or at least to establish to which extent it can be valid. Even if it could also provide information on the necessary array size, experience showed that the size of seismic deployments (arrays) in urban areas is generally limited by practical constraints such as main transportation lines or changes in the topography and surface geology. *A priori* information is also necessary to provide constraints on subsequent inversions in terms of realistic material properties and eventually depth of interfaces, especially the bedrock/sediment interface. For that purpose, geological and topographical maps and results from previous boreholes and geophysical experiments were collected. Table 1 lists all stations installed during this project along with the measurements performed (passive and active) at each site and the surface geology. Within the project, 27 array measurements with 60 to 480 m aperture and about 10 m minimum interdistance were performed. In addition, two existing passive measurements were reprocessed, and four MASW experiments were performed (typically 50 m long geophone linear arrays with 1–2 m interstation distance). The passive array measurements were typically made with 14 Lennartz 3C-5s seismometers data were acquired using Quanterra Q330 digitizers. An example of array setup for the site SBUH, with a large aperture, is shown in Figure 4. Two-hour recordings of 1–2 array layouts (rings of 3–5 stations with increasing radius around a central station) were made. In some cases, the recordings were made at night to minimize nearby noise sources. The MASW experiments were performed either using a sledgehammer or weight drop (120 kg) as active source, with data acquired on geophone strings and, in a few cases, seismological stations.

Following the acquisition of ambient vibration data, the following processing steps are applied to each dataset:

Table 1
Overview of the 30 Stations Installed during the Project and Their Site Properties Sorted by V_{S30}

Station Code	Name	Start Date (yyyy/mm/dd)	Meas.*	Site	Type	Resonance Frequency			Travel-Time Average *S*-Wave Velocity					
				Surface Geology	EC8	f_0	Interpretation	Depth (m)	V_{S10}	V_{S30}	V_{S50}	V_{S100}	V_{S200}	EGSW†
SLUW	Luzern Werkhofstrasse	2010/12/23	P+A	Reclaimed land	C	1.15	Quaternary (unclear)	200	154	224	275	365	504	Yes
SEPFL	Lausanne-EPFL	2011/10/26	A	High terrace (Pleistocene)	C	1.9	Quaternary (1D)	37	162	224				
SYVP	Yverdon-Philosophes	2011/09/07	P	Spit (Holocene)	C	1.15	Quaternary (1D)	80	194	257	279	353		Unclear
SINS	Interlaken	2012/09/17	P	Alluvia (Holocene)	C	0.51	Quaternary (2D)	380	202	266	313	371	455	Yes
SOLB	Solothurn Brühl	2011/11/22	P	Alluvial fan (Holocene)	C	0.6	Quaternary (unclear)	180	185	274	326	396	479	Yes
SLOP	Locarno Pompieri	2013/06/24	P	Alluvial fan (Holocene)	C	0.67	Quaternary (1D)	450	271	304	339	400	503	
SIOM	Sion-Mayennets	2011/01/06	P	Alluvial fan (Holocene)	C	0.46	Quaternary (2D)	150	351	365	432	504		Yes
SBERN	Bern Kleine Schanze	2013/06/07	P	Reclaimed land on moraine (Pleistocene)	C	2	Quaternary (1D)	40	254	366	433	567		
SBRS	Brig Spital	2012/09/03	P	Alluvial fan (Holocene)	C	1.4	Quaternary (unclear)	200	234	386	492	627	788	Unclear
SGEV	Genève-Vieux Billard	2011/12/13	P	Alluvia (Holocene)	B	4.2	Quaternary (1D)	24	286	415	562			
SBUH	Buchs-Hochschule	2012/10/22	P	Alluvia (Holocene)	B	0.6	Quaternary (1D)	250	301	420	360	380	465	Unclear
SOLZ	Solothurn Zeughaus	2012/01/18	P	Moraine (Pleistocene)	B	1.45	Quaternary + Tertiary (1D)	170	315	432	473	557		
STGK	St Gallen Klosterhof	2012/03/16	P	Moraine (Pleistocene)	B	4	Quaternary (1D)	40	241	440	577			
SBEG	Bettingen-Gewerbehaus	2012/02/13	P	Alluvia (Holocene)	B	4	Quaternary (1D)	35	346	444	575			
SALTS	Altdorf Spital	2012/11/12	P	Alluvial fan (Holocene)	B	1.2	Quaternary (1D)	320	359	470	524	656	829	
SVAM	Vaz-Muldain	2011/05/26	P	Flysch (Upper Cretaceous–Eocene)	B	4	Unstable slope (1D)	45	310	486	582			
SNIB	St Niklaus Bahnhofstrasse	2010/12/13	P	Alluvial fan (Holocene)	B	1.3	Quaternary (2D)	>100	443	505	540	706		Unclear
SRER	Reinach-Rainenweg	2011/05/16	P	Low rubble terrace (Pleistocene)	B	0.45	Quaternary + part of Tertiary (1D)	>570	474	514	557	613	788	Yes
SAIG	Aigle-rue de la Gare	2012/04/20	P	Alluvial fan (Holocene)	B	1.4	Quaternary (unclear)	350	420	535	587	777	1009	Unclear
SARK	Sarnen Kantonsschule	2012/05/30	P	Alluvia (Holocene)	E	2.3	Quaternary (1D)	160	307	541	709	939		
SMAO	Martigny Octodure	2012/11/12	P	Alluvia (Holocene)	B	0.85	Quaternary (unclear)	250	349	567	677	796	882	Unclear
SGRA	Grächen Ausblick	2010/12/13	P	Moraine	B	0.7	Unstable rock slope (1D)	500	398	576	694	878	1094	
SZUZ	Zürich Zeughaushof	2012/12/19	P	Gravels of the Sihl river (Pleistocene)	B	0.93	Quaternary + part of Tertiary (1D)	250	372	579	656	651	746	
SBUA2	Buchs-Altendorf	2011/08/17	P	Alluvial fan (Holocene)	B	3.6	Quaternary (2D)	90	405	618	771	1025		Unclear
SLTM2	Linthal-Matt2	2011/05/31	P	Slope waste (Holocene)	B	1.34	Quaternary (unclear)	250	468	620	723	876	994	
SCUG	Chur Gewerbeschulhaus	2011/18/11	P	Alluvial fan (Holocene)	B	0.46	Quaternary (2D)	700	516	714	825	960	1119	Unclear
SIEB	Sierre Ecole de Borzuat	2012/05/11	P	Slope loam (Holocene)	B	2.4	Quaternary (1D)	200	492	726	818	1015		
SCHS	Schaffhausen-Spital	2011/06/09	P	Moraine (Pleistocene)	A	12	Quaternary (1D)	15	646	960	1190			
SLUB	Luzern Bramberg	2011/12/02	P+A	Sandstone (Marine Molasse, Tertiary)	A		No resonance		711	1100	1426			
SBUB	Buchs-Buchserberg	2010/09/02	P+A	Limestone (Cretaceous)	A		No resonance		871	1563				

*P, Passive array measurement; A, active seismics-MASW
†Edge-generated surface waves

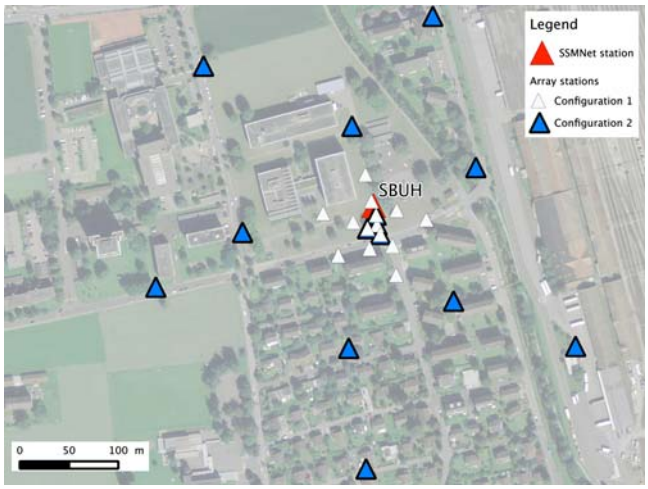

Figure 4. Array setup for site SBUH. The color version of this figure is available only in the electronic edition.

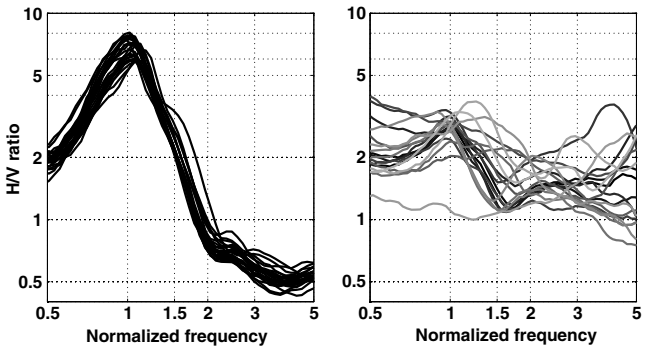

Figure 5. H/V analysis of array points of sites SBUH and SBUA2 using time–frequency analysis (Poggi *et al.*, 2012). The frequency axis has been normalized by the resonance frequency of the site.

1. Single-station analysis through H/V spectral ratios and polarization analysis. The former are used to retrieve the fundamental frequency of resonance and—to some extent—the ellipticity of the fundamental mode of Rayleigh waves. The latter might indicate evidence of 2D resonance or unstable rock slopes.
2. Array analysis to retrieve the dispersion curves of Love and Rayleigh waves.
3. Combined inversion of dispersion, resonance, and ellipticity curves.

Each step is detailed hereafter and summarized in Figure 3.

Before any processing on the stations of the array, data quality is ensured in time and frequency domains to detect the presence of signal disturbances or vibrating structures. The orientation of the sensors is checked following the optimization procedure described in Poggi *et al.* (2012): the correlation of signals at low frequencies is used to detect the misorientation of sensors in the horizontal direction that can affect subsequent 3C processing. A correction is subsequently performed with respect to a reference station. Because a compass is used in the field to orient the instruments, errors up to 10° are commonly found, but larger errors might occur when sensors are placed close to disturbances of the magnetic field. H/V analysis of each recording of the array and other available recordings in the area is then performed using different approaches to ensure the quality of the results. In particular, methods based on time-frequency analysis are, at least theoretically, able to remove the Love-wave contribution on the horizontal components (Fäh *et al.*, 2009; Poggi *et al.*, 2012) and were therefore preferred to analyze Rayleigh-wave ellipticity functions. H/V spectral ratios are initially used to ensure the homogeneity of the measurement area (1D assumption) is fulfilled and, second, to estimate the fundamental mode of Rayleigh-wave ellipticity function and the fundamental frequency of resonance at the site. Maps of the fundamental frequencies (f_0) were produced to understand the variability of the geology in the area of the seismic station. Figure 5 shows the example of a homogeneous site (SBUH, located on a large alluvial plain) and a site with strong lateral variability (SBUA2, located on an alluvial fan).

Following the computation of spectral ratios, single-station wavefield polarization analysis is performed using the approach of Burjánek *et al.* (2010). It provides, at each frequency, the azimuthal distribution of the energy of the ground motion and the parameters of the ground-motion ellipse. Pronounced ellipticity and focusing of ground motion in a particular azimuth are searched for throughout the array. Such effects may be interpreted as a 2D resonance of the structure if observed throughout the array. In case of identified 2D resonances, the ellipticity information is not used for the inversion of the 1D velocity profile because 1D theory of Rayleigh-wave propagation does not hold anymore around the frequencies of the 2D resonance. This is discussed in more detail in the last paragraph of this section.

For the array processing, high-resolution frequency–wavenumber (HRFK) analysis (Capon, 1969) on the vertical component is first performed using the software package Geopsy for ensuring quality (Wathelet *et al.*, 2008). Subsequently, 3C HRFK analysis following Fäh *et al.* (2008) and Poggi and Fäh (2010) is performed. Compared with the computation on vertical components only, 3C analysis makes optimal usage of the available channels to estimate, in addition, the dispersion of Rayleigh waves in the radial direction of propagation and of Love waves. Moreover, it allows the computation of the ellipticity function of Rayleigh waves. Figure 6 shows the 3C HRFK analysis performed to characterize the station SBUH.

For few difficult sites, such as those with very stiff soil and rock, active seismic experiments were also performed. The active source provides coherent energy at high frequency that in many cases is lacking in the ambient vibration wavefield. As a drawback, however, the maximum depth resolution is generally limited to about 30 m. MASW processing includes the standard f-k technique (Park *et al.*, 1999) and the wavelet-based method of Poggi *et al.* (2013) to derive Rayleigh- and eventually Love-dispersion curves at high

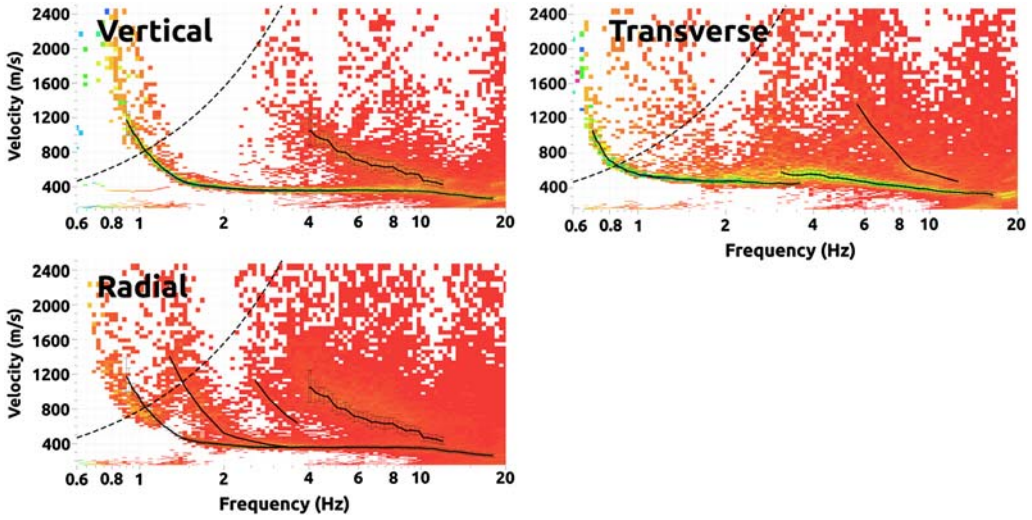

Figure 6. Three-component high-resolution frequency–wavenumber (3C HRFK) analysis (Poggi and Fäh, 2010) of an array around SBUH station. The dashed lines indicate the lower resolution limit of the array. The black lines indicate the selected dispersion curves with their uncertainty when available. The radial component highlights Rayleigh-wave higher modes that cannot be seen on the vertical component. The transverse component provides Love-wave modes. The color version of this figure is available only in the electronic edition.

frequencies, depending on the sensor availability (vertical or three component). The latter approach is particularly advantageous in use with continuous data from the seismological equipment of passive seismics. In some cases, other than just surface waves, head waves have been observed from f-k analysis, which are useful to constrain the presence of shallow but large velocity contrasts.

Finally, all available information (Love and Rayleigh dispersion, ellipticity curves, and fundamental frequency of resonance) is inverted into a set of 1D velocity profiles using a direct search approach (global optimization) based on the modified neighborhood algorithm (Wathelet, 2008). A certain level of interpretation is needed for the input data before being inverted. As first, only the portions of the dispersion curves that lie within the array aliasing and resolution limits are considered (Wathelet *et al.*, 2008). From the ellipticity curve (H/V curve), only the right flank of the fundamental peak was generally used, because ellipticity can be identified best in this frequency range and contains information about the soil structure (Fäh *et al.*, 2001; Hobiger *et al.*, 2012). Extracted sections of dispersion curves are then compared and interpreted as fundamental or high-order modes (mode addressing). The interpretation can change during the procedure if new evidence arises, for example, in support of alternative modal patterns.

The resulting profiles are discrete representations of the elastic properties of the ground (V_P, V_S, and density). Each profile is represented by a series of homogeneous horizontal layers. Given the highly nonlinear nature of the inversion problem to solve, additional *a priori* geological and geotechnical information are required to define the bounds of the search and consequently to restrict the size of the parameter space. This is useful to avoid unrealistic solutions due to overfitting (Wathelet, 2008) and trapping in local minima of the misfit function. When available (in rare cases), borehole information was used to fix the depth of interfaces (e.g., at SEPFL site). Moreover, conditional constraints are often used, such as increasing velocity with depth (except if geology or particular characteristics in the dispersion curves suggest the presence of specific low-velocity layers) and realistic V_P/V_S ratios. For the latter, the Poisson's ratio is generally kept in the 0.2–0.4 range, although higher values were allowed just below the water table, where the V_P/V_S ratio can be rather large. Density values are fixed *a priori* based on the available local information (borehole data or literature); in practice, realistic changes in density have little impact in terms of amplification. Two different layer thickness schemes are used jointly, allowing fixed and free-layer interface depths. Using the fixed scheme has the advantage of reducing the nonuniqueness of the inversion problem but might lead to smooth velocity profiles. Conversely, a free-layer approach is very nonunique and might require considerable *a priori* information but lead to a better resolution of sharp velocity interfaces. An example of combined inversion of dispersion curves and ellipticity for station SBUH is presented in Figure 7.

A major issue related to the inversion of surface-wave data is the estimation of uncertainty in the results. Uncertainties are due to measuring errors such as the inaccurate picking of dispersion curves; and due to the forward modeling of surface-wave dispersion assuming a 1D velocity model with a limited number of layers. Because it is difficult to determine and represent the probability function in a space with many dimensions, the uncertainty was reflected by selecting a number of realistic profiles. This is done by performing the inversion on different parameterization schemes (free- and fixed-layer depths) and multiple inversion attempts using variable initial randomizations of the parameter space to be searched. Although this does not ensure the whole range of

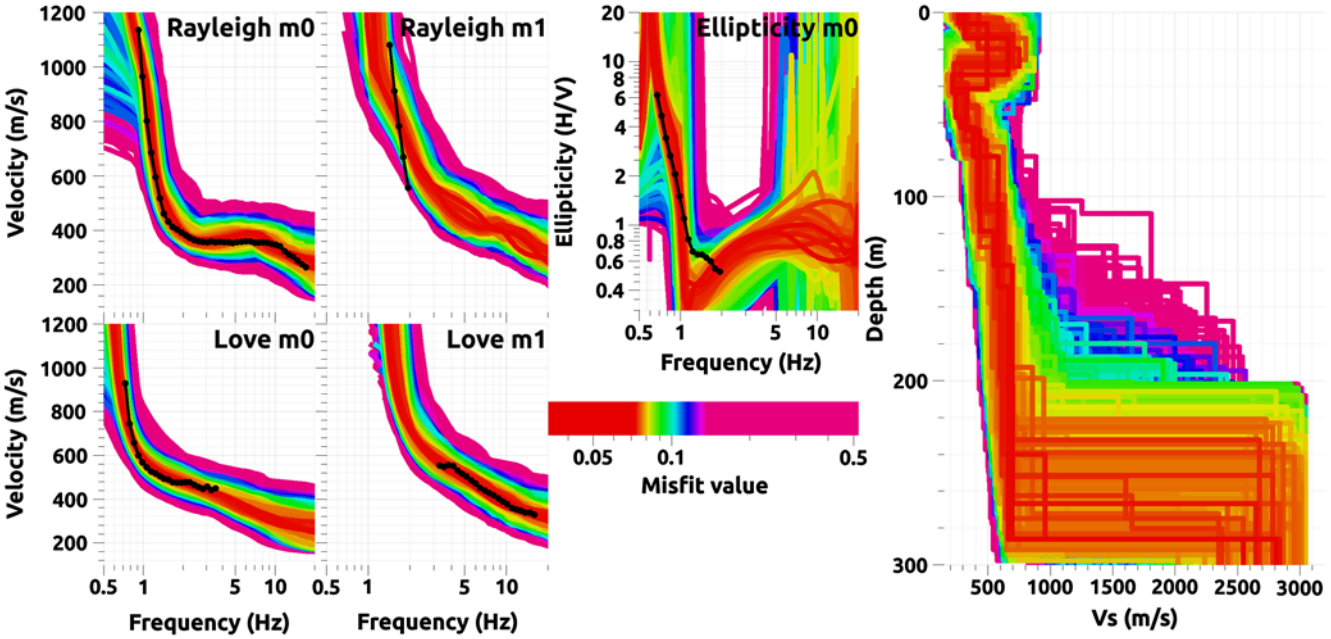

Figure 7. Combined inversion of dispersion curves (two modes of Rayleigh waves, two modes of Love waves) and right flank of the ellipticity of Rayleigh waves into velocity profiles (only V_S presented here). The black dotted lines indicate the observed properties, whereas the background lines indicate the inverted properties. The scale, denoting the misfit value, is consistent across the different plots. The color version of this figure is available only in the electronic edition.

uncertainties is covered, it nevertheless provides a homogeneous procedure to estimate the uncertainty to some extent.

From the selected 1D velocity profiles, several engineering parameters are derived along with their uncertainty. These parameters are the ground type, based on EC8 classification (Eurocode 8, 2004), travel-time average velocity at different depths (e.g., 5, 10, 20, 30, 50, 100 m) and frequency-dependent parameters: quarter-wavelength velocity (Joyner *et al.*, 1981), quarter-wavelength impedance contrast (Poggi, Edwards, and Fäh, 2012), and *SH*-wave transfer function for vertical incidence.

Comparison with Spectral Modeling

The site characterization undertaken for this project was based on well-established methods. However, to check the validity of the obtained velocity profiles, a comparison with amplification function from empirical spectral modeling (ESM) of earthquake ground motion at the permanent stations was performed. This technique has been described in detail by Edwards *et al.* (2008, 2013), with a similar approach shown by Thompson *et al.* (2012) to be able to distinguish non-1D effects. Each event detected by the seismological network is analyzed in near real time. The spectra of all recordings with sufficient signal-to-noise ratio are inverted to obtain the source parameters using a model for the path and known reference rock condition. The residuals at each station are interpreted as the site terms (Edwards *et al.*, 2008). Statistics over many small events allow convergence to a stable site amplification function, hereafter called ESM function, and its uncertainty. A region-dependent geometrical spreading of Edwards and Fäh (2013) was implemented instead of the classical $1/R$ decay. This allows us to avoid potential biases in the spectral estimation in particular in the near field. The ESM function describes the elastic amplification with respect to the Swiss reference rock velocity model (Poggi *et al.*, 2011). Therefore, it can be compared with 1D *SH* transfer function from site characterization after a correction from the reference rock, as shown by Edwards *et al.* (2013). This approach was systematically used here to check the validity of the 1D velocity profiles. The agreement between the two curves is checked relative to the presence of peaks, their frequency values, and the level of amplification. This comparison is performed keeping in mind that expected differences may occur; non-1D wave propagation phenomena such as EGSW or 2D/3D resonance cannot be reproduced by 1D transfer functions. Furthermore, there are potential trade-offs in the spectral inversion between elastic amplification and anelastic attenuation that may lead to incorrect amplification levels at high frequencies. The comparison between theoretical 1D-*SH* and ESM amplification led to a reinterpretation of the dispersion curves, and consequently to a new inversion for velocity profiles, in which significant differences were apparent.

An example of the *SH* versus ESM amplification comparison is presented in Figure 8 (station SBUH) in which the first inversion (without low-velocity zone) led to acceptable fit of the dispersion curves, but the empirical and theoretical amplification functions were not matching. Subsequently, allowing for a low-velocity zone close to the surface led to models that better reproduce the empirical amplification function. The low-velocity zone is due to the presence of fine uncompacted sediments below a gravel layer and was

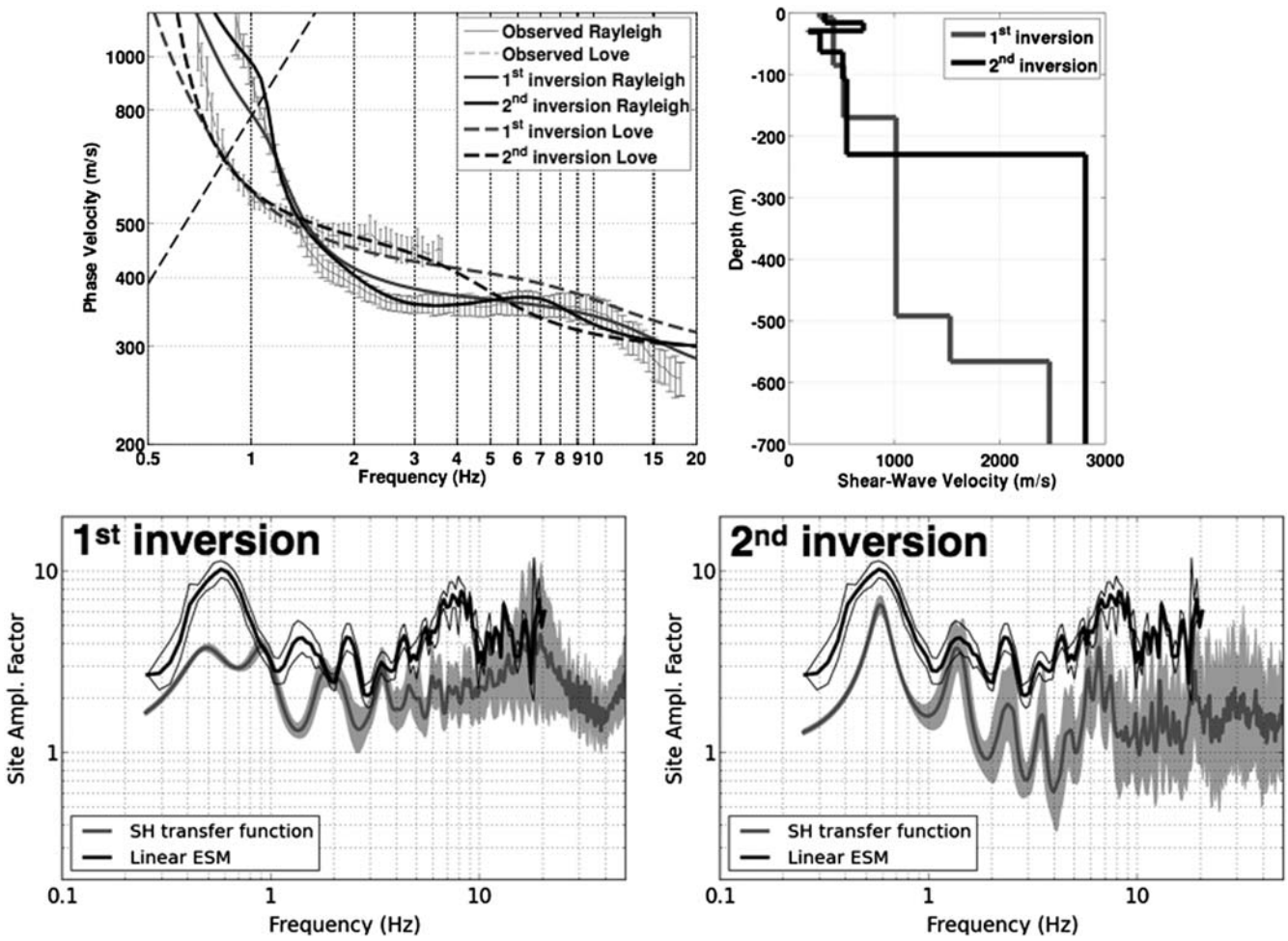

Figure 8. Comparison between the first inversion performed without velocity inversion and the second that allows a low-velocity zone. Top left: dispersion curves (fundamental Love and Rayleigh) of one selected model of each inversion and observations with error bars. Top right: selected models for each inversion. Bottom: comparison of ESM amplification and *SH* transfer function for each inversion.

confirmed by borehole analysis. Apart from the low-velocity zone close to the surface, the initial and adjusted velocity models are similar in the first 150 m. The bedrock depth, constrained only by the H/V peak, is also considerably different. This shows the difficulty to obtain reliable profiles beyond the depth constrained by the dispersion curves, even using the ellipticity. To estimate the depth where the profile is resolved, the quarter-wavelength approach can be used (Joyner *et al.*, 1981). For given velocity profiles, it can provide an estimate of the depth corresponding to the lowest frequency in the dispersion curves (0.85 Hz—corresponding to 120 m depth for the case in Fig. 8). However, this value is relatively rough and conservative.

Detection of 2D/3D Effects

To detect 2D resonance in our site characterization procedure, we used polarization analysis following the technique of Burjánek *et al.* (2010). This approach uses single-station processing of array data and assumes that a strong polarization in the valley axis is an indication for 2D resonance (Ermert *et al.*, 2014). Moreover, this procedure can highlight 2D/3D effects in case of sites with pronounced topography (Burjánek *et al.*, 2012, 2014). The procedure outlined in this article aims to classify the sites of the stations (i.e., existence of 2D/3D effects). More investigations are necessary to better understand the 2D/3D behavior but are beyond the scope of this study.

The detection of EGSW is based on the comparison of the theoretical 1D-*SH* with the ESM amplification. The level of amplification of 1D models, and therefore of the aggravation factor (Cornou and Bard, 2003), is largely controlled by the bedrock velocity, which is generally uncertain. It may therefore be difficult to know whether deviations from observed amplification functions are due to unknown bedrock velocity at depth or 2D/3D effects. Nevertheless, by comparing the ESM amplification function, which integrates all geometrical (1D, 2D, 3D) effects, with the 1D-*SH* transfer function from the site characterization, we identified characteristic deviations in shape (peaky versus smooth functions) where EGSW were suspected. The classification of sites exhibiting EGSW was therefore objectively assessed based on the comparison of amplification shape rather than amplitude.

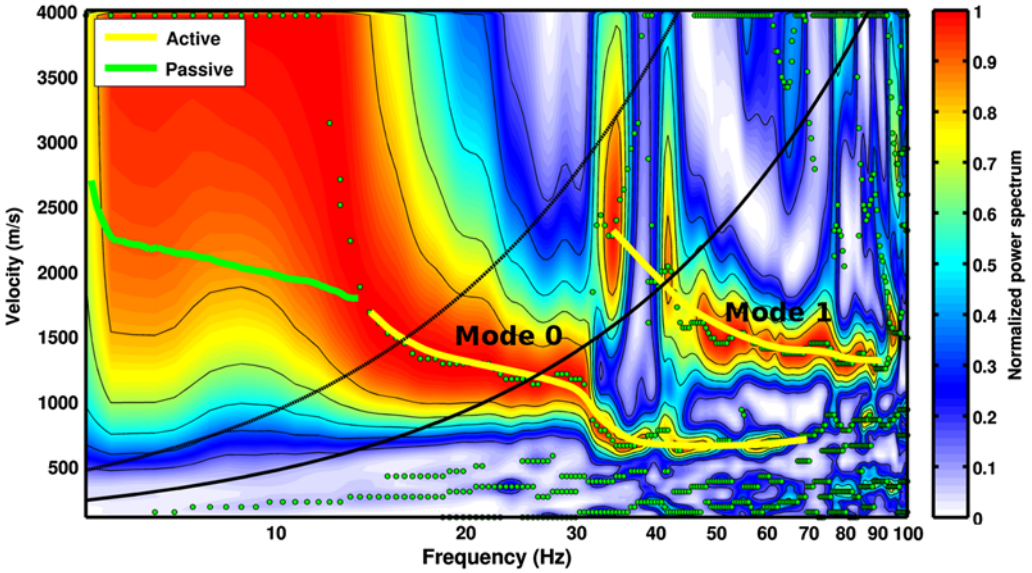

Figure 9. Multichannel analysis of surface wave (MASW) analysis at site SLUB (vertical component) with interpretation of Rayleigh-wave fundamental and first higher modes. The dispersion curve retrieved from the passive measurement is also displayed. The black bended line is the resolution limit of the MASW analysis. The color version of this figure is available only in the electronic edition.

Results from 1D Site Characterization

Table 1 summarizes the results of the site characterization. The resonance frequencies across all sites range from 0.45 to 12 Hz. Using the combined inversion, the resonance frequencies are interpreted as the resonance of the soil column above an interface at a given depth (Table 1). The 30 sites range therefore from very deep sedimentary sites (down to 600 m depth) to shallow sediments (15 m depth) and rock sites (no resonance or at high frequency). Most of the time, particularly in the Alpine area, the fundamental frequency corresponds to the interface between sediments and the bedrock. At some sites, it has been clearly shown that the resonance frequency is related to 2D resonance of the whole basin (see Classification of Sites with Respect to 2D/3D Response section). In three cases (SOLZ, SRER, and SZUZ), all located in the Swiss foreland, the observed resonance corresponds to layers including Tertiary sediments. This fact was already recognized in previous studies concerning the region of Basel (station SRER, e.g., Steimen *et al.*, 2003). In two other cases on alpine rock slopes, the resonance may be related to slope instability. This has been already shown for the Grächen case (SGRA) (Fäh *et al.*, 2012) but needs more investigation for the site Obervaz (SVAM).

There is no doubt that the resulting velocity profiles benefit from the 3C array analysis technique because more information is retrieved: in particular the transverse component allows the retrieval of Love dispersion curves and the radial component sometimes better outlines the higher Rayleigh-wave modes than vertical-component analysis only. Misinterpretation of mode addressing can also be minimized leading to more robust and accurate inversions. This is illustrated in Figure 6: on the radial component, the first and second Rayleigh-wave higher modes appear, although they could not be seen on the vertical component. The third higher mode may have been mistakenly interpreted as the first by looking at the vertical component only. At only two sites could no dispersion curves on the transverse component be observed: SLUW in the deep lacustrine basin of Lucerne (Poggi *et al.*, 2012) and SIOM in the Rhône valley (Roten *et al.*, 2006). This may be due to the absence of a velocity gradient in the basin, or at least one that is not very pronounced, because Love waves do not propagate at the surface of a homogeneous half-space.

Active seismics, particularly MASW, proved to be complementary to ambient vibration arrays (Poggi *et al.*, 2013). Their combined use was helpful in the case of the rock site SLUB (Fig. 9). A 46 m string of 24 geophones was used together with a weight of 120 kg dropped from 1.1 m height. The upper 15 m were constrained by the active experiment, whereas the bottom part until 75 m depth was retrieved using a passive array of 160 m aperture. Unfortunately, none of these techniques provided good results on the hard-rock site SBUB, where it was necessary to employ refraction seismics.

According to the comparison with ESM, a revision of 13 out of 30 sites was performed. This large number is partly due to the low amount of previous knowledge of the sites. The main reasons that led to incorrect profiles, and therefore mismatch with the ESM amplification, were errors in mode assignment, overconfidence in the H/V function as proxy for the ellipticity, and unnoticed low-velocity layers at depth. Mode assignment has already been detected as an issue by Cornou *et al.* (2009) after an international blind test. The interpretation is especially difficult at osculation points, that is, where two modes are very close to each other. Moreover, even if some sections of H/V curve are in many cases a good proxy for the Rayleigh-wave ellipticity, many authors showed it may be biased by the Love-wave contribution and non-1D effects (Fäh *et al.*, 2001; Bonnefoy-Claudet *et al.*,

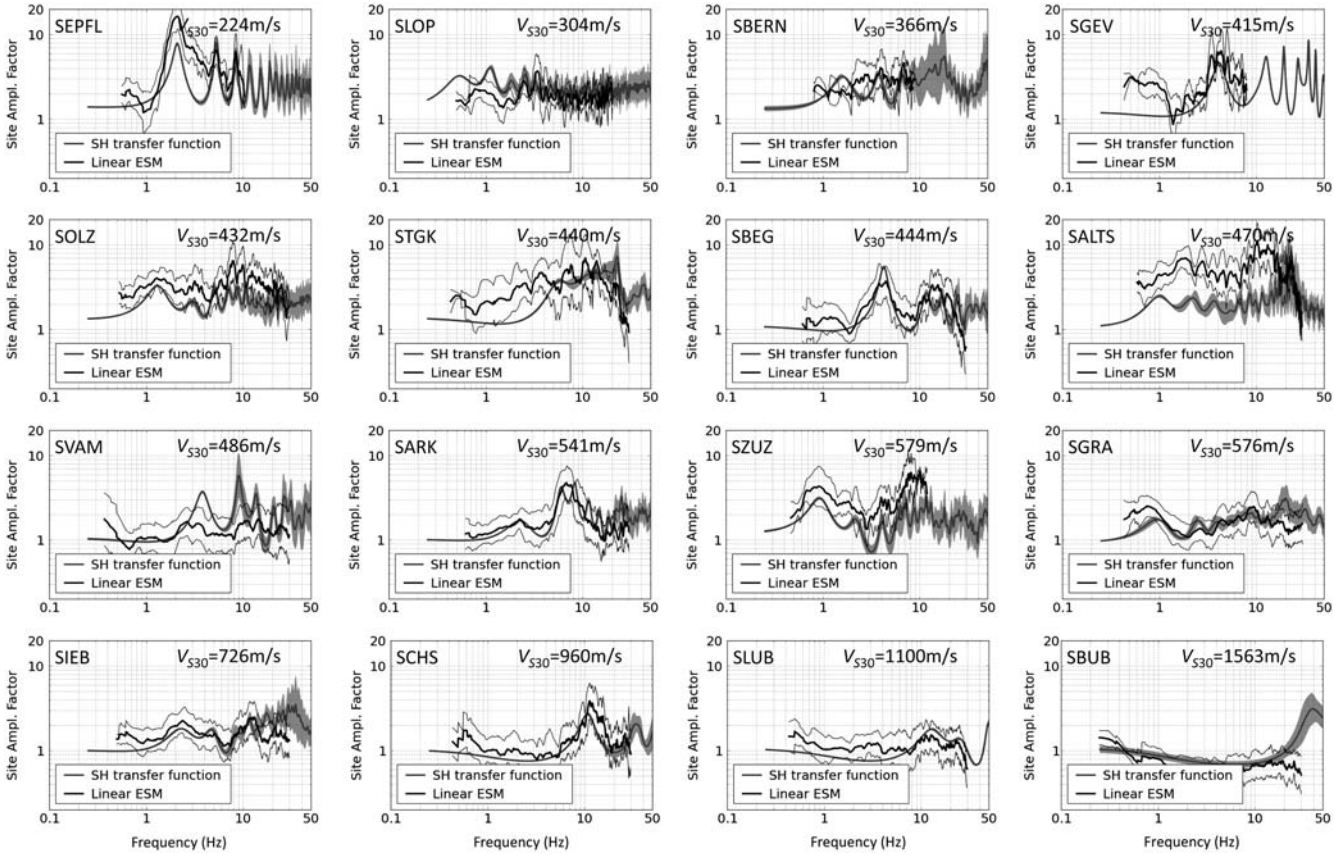

Figure 10. Comparison between *SH* transfer function from site characterization and ESM elastic amplification for 1D sites ordered by increasing V_{S30}.

2006). In our procedure, Love-wave contribution to the H/V ratio was minimized using time–frequency analysis (Poggi *et al.*, 2011) and 3C array analysis (Poggi and Fäh, 2010). Finally, as explained in the previous section, low-velocity zones were considered only if no model with increasing velocity with depth could be found that explains the observations. Surface-wave analysis alone in general is not robust enough to reliably resolve low-velocity zones. A comparison with ESM amplification and complementary data (borehole information, when available) should therefore be used.

It should be underlined that the comparison process does not ensure that profiles are unbiased, even in 1D cases. There are trade-offs between different parameters in the inversions that cannot be tested through this comparison. For instance, the inversion of bedrock depth and velocity at depth, where no dispersion curve is available, is generally nonunique and relies on the H/V curve that may not always represent the ellipticity of the fundamental-mode Rayleigh wave. However, the comparison with empirical amplification helps reduce the bias on the estimated velocity profiles.

The comparison of the retrieved velocity profiles for 1D sites is presented in Figure 10. The 1D profiles are particularly good at representing the elastic amplification at each site. Other sites are treated in the next section.

Figure 11 presents the V_{S30} of all sites with respect to the maximum amplification value in the ESM function in the frequency band 1–10 Hz. It shows the clear correlation between V_{S30} and amplification but is particularly useful to show the range of these two parameters. This figure shows the majority of sites are categorized as ground type B (stiff sediments). This is due to the fluvial-glacial nature of a large part of the alpine sediments. They cause amplification with respect to the Swiss reference of a factor 1.7–8. Glacial-lacustrine sediments are also present (six sites) and correspond to ground type C with V_{S30} values from 220 to 300 m/s. Their maximal amplification is between 4 and 17. No site belongs to ground type D ($V_{S30} < 180$ m/s). Three rock sites have been instrumented with very different characteristics such as a hard-rock site in the Alps (SBUB), a site on molasse rock in the Foreland (SLUB), and a hard-rock site in the Jura zone overlain by a thin consolidated moraine layer (SCHS). SLUB is comparable to the Swiss reference velocity model, whereas SBUB shows deamplification and SCHS amplification up to 30%. Only one site (SARK) falls in the EC8 definition of ground type E (thin layer of C or D ground type on rock).

Classification of Sites with Respect to 2D/3D Response

Figure 12 classifies the different sites with respect to the presence of EGSW and 2D/3D resonance (see also

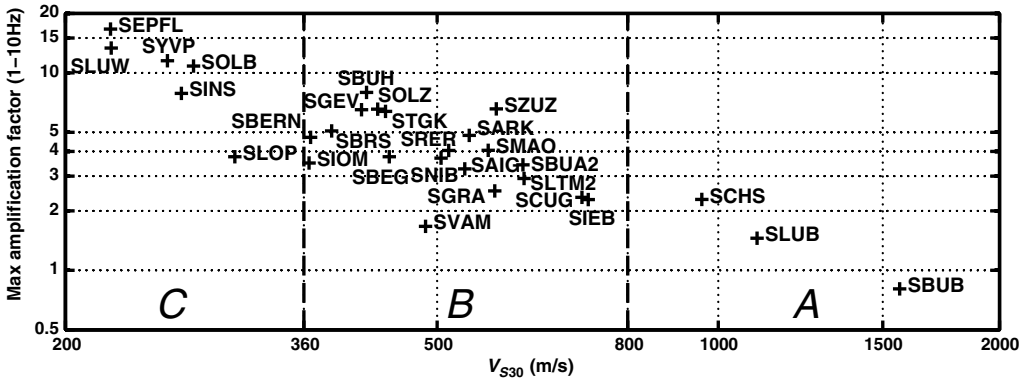

Figure 11. Distribution of the station sites with respect to V_{S30} and maximum amplification in the ESM function in the 1–10 Hz frequency band. Definition of A, B, and C ground types of EC8 (Eurocode 8, 2004), based on V_{S30}, are also displayed.

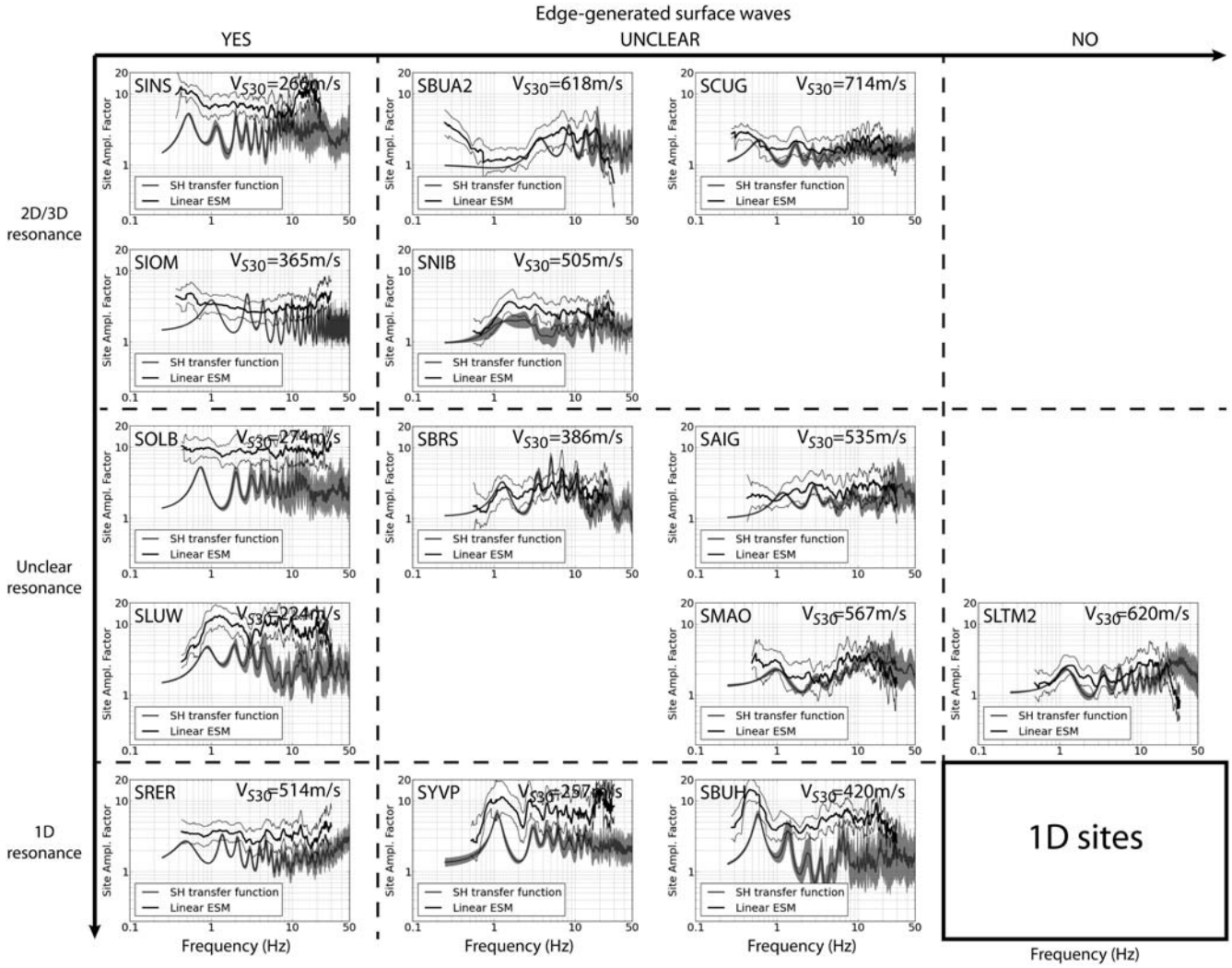

Figure 12. Comparison between *SH* transfer function from site characterization and ESM elastic amplification for sites with clear or possible 2D/3D effects. Horizontal axis: classification of edge-generated surface waves (EGSW) using the level of agreement of the ESM with the theoretical 1D response (from left to right: presence of EGSW, unclear case, and no EGSW); Vertical axis: classification of 2D/3D resonance using the polarization analysis comparison (from top to bottom: 2D/3D resonance, unclear case, and 1D resonance).

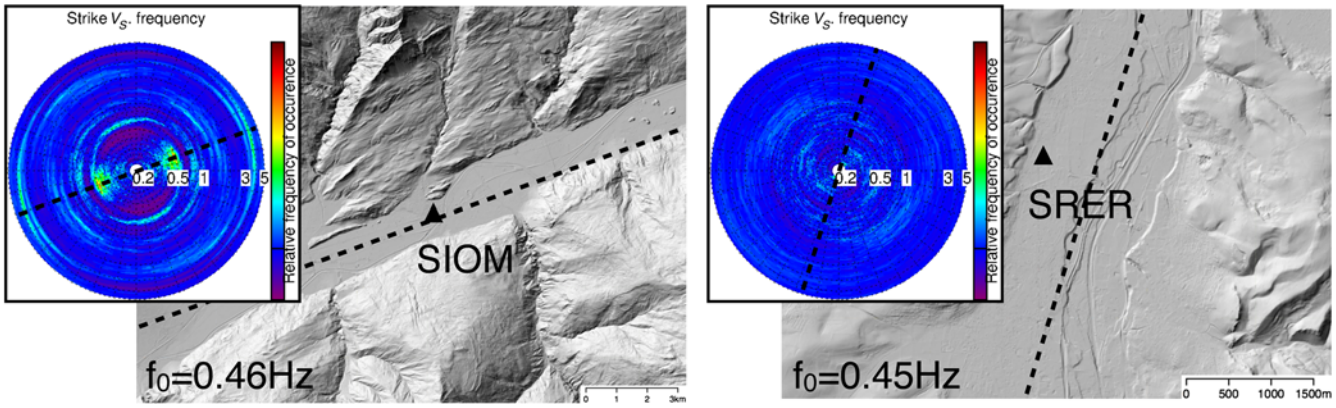

Figure 13. Polarization analysis of sites SIOM (2D/3D resonance with EGSW) and SRER (1D with EGSW) and topographic map of the sites. Dashed black lines are showing the valley axis of each site and are reproduced on the polar plot. The polar plots represent the azimuthal distribution of the energy for frequencies between 0.2 and 5 Hz. The color version of this figure is available only in the electronic edition.

Table 1). Clear 1D sites are excluded from this figure and are presented in Figure 10. EGSW can be observed at sites SIOM, SINS, SOLB, SLUW, and SRER. Even if the velocity contrasts are not so large, the difference due to EGSW at site SRER is clear. Their presence at some other sites cannot be excluded. These sites are therefore classified as unclear. For instance, at SCUG, the velocity contrasts are low so that the smooth shape of the amplification function cannot be clearly attributed to these low contrasts or EGSW. At station SBUA2, the smooth part between the first and second peak in the ESM function is likely to be related to EGSW. A more detailed characterization of this effect requires a 2D parameterization of the sites and numerical modeling (Paolucci and Morstabilini, 2006) that will be performed in future studies.

Five sites show a clear polarization of the wavefield at the resonance frequency in the expected direction of a 2D resonance. Sharp peaks in the spectra, related to industrial activities and polarized in the direction of the source, were excluded from the analysis. SIOM, SINS, and SCUG are located in the deeply filled valleys of the Rhône, Aare, and Rhine rivers, in the Alpine area, respectively. At their fundamental frequency of resonance, the wavefield is polarized along the valley axis, corresponding therefore to the fundamental *SH* mode (e.g., Fig. 13 for SIOM station). More refined studies should be applied to array recordings along cross section to detect the other resonance modes (e.g., Roten *et al.*, 2006; Ermert *et al.*, 2014). SBUA2 and SNIB are located in much smaller structures, namely an alluvial fan on the side of the Rhine valley and the small alpine valley of the river Mattervispa (Fritsche *et al.*, 2005). Both sites clearly show a polarization in the axis of these structures at the resonance frequency. For several other sites, polarization could be detected but was either weak (e.g., SOLB) and/or in a direction not corresponding to the main valley axis. For stations SLTM2 and SAIG, the polarization at the resonance frequency is perpendicular to the valley axis. They are both located on alluvial fans that may influence the wavefield, but their small sizes compared with the whole valley may indicate that the fundamental *P-SV* mode is observed. These sites are nevertheless categorized as unclear in Figure 12. Moreover, at some sites like SRER, no particular polarization of the wavefield could be noticed (Fig. 13), and these sites are therefore classified as exhibiting 1D resonance.

A further indication of 2D/3D resonance is given by the shape ratio and velocity contrast of the considered 2D structure, as shown by Bard and Bouchon (1985). The shape ratio is defined for sine-shaped valleys as the ratio of maximum sediment thickness h to the valley half-width l. Bard and Bouchon (1985) also defined an equivalent shape ratio for any other valley type as $h/2w$, with 2w the total width over which the sediment thickness is greater than half its maximum value. The velocity contrast is computed as the ratio of the bedrock *S*-wave velocity to the travel-time average *S*-wave velocity of the sediments layers. The bedrock velocity and shape ratio are sparsely known in our project because we were focused on 1D and not 2D geometry. However, at many sites, these values could be estimated, sometimes with a large interval of uncertainty, and are displayed in Figure 14. These results are in agreement with the conditions defined by Bard and Bouchon (1985) for the critical curve, because sites on the right part of this curve were already identified as exhibiting 2D/3D behavior, taking the uncertainties into account. Unclear sites are mostly located close to the critical curve. SOLB and SLUW, based on this figure could eventually be reclassified as 1D resonance sites with EGSW. Sites recognized without 2D/3D resonance are located on the left part of the plot as predicted by Bard and Bouchon (1985). These authors also clearly state that the transition is smooth from 1D to 2D behavior and that the critical curve is in reality more blurred, which is also consistent with the results found here. Unclear sites may therefore be renamed as "transition" sites but may never be classified exclusively in 1D or 2D/3D resonance categories.

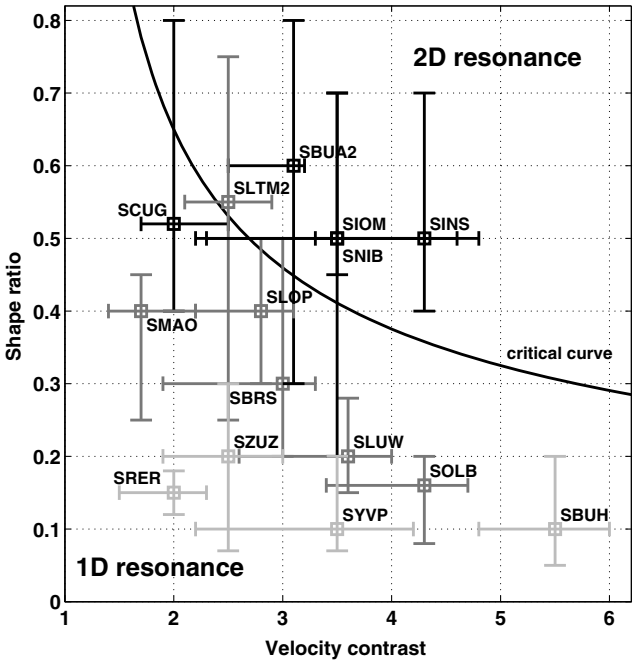

Figure 14. Shape ratio as a function of velocity contrast for a selection of studied sites (squares with uncertainty intervals) and proposed critical curve (black line) from Bard and Bouchon (1985). Site classification with respect to resonance from Figure 12: 2D (black), unclear (dark gray), and 1D (light gray).

Finally, 2D/3D effects are most significant at sites SIOM and SINS with clear 2D resonance and EGSW. At eight other sites, resonance and/or EGSW are considered as unclear, but 2D/3D effects are present. EGSW are sensitive to geometry and velocity contrasts at the basin edges (locally), whereas 2D/3D resonance is a global phenomenon and therefore depends on average parameters (geometry and elastic properties) of the whole geological structure. For instance, at site SRER in the Rhine graben, steep normal faults at the basin edge generate EGSW, but the basin is too flat to generate 2D resonance (Steimen *et al.*, 2003). However, in the case of alpine valleys such as the upper Rhône, Rhine, and Aar valleys, more regular, EGSW and 2D resonance are more likely to occur together.

Conclusions

In the framework of the SSMNet renewal project phase 1, we proposed and systematically applied a site characterization procedure based on surface-wave analysis, particularly using ambient vibrations. A method based on spectral modeling was used to check the validity of the retrieved 1D velocity profiles. Despite the relevance of the collected data and their analysis, this comparison procedure led to numerous reinterpretations, strongly contributing to an increase in the quality of the results. Such a comparison procedure can therefore be recommended for future projects.

The whole procedure allowed the detection of non-1D effects, namely 2D/3D resonance using polarization analysis and EGSW using the comparison between 1D transfer function and ESM amplification. It has been found that a 1D assumption was valid and sufficient to represent the ground response to seismic motion in many of the studied cases. However, field measurements are absolutely necessary to extract 1D profiles representative of the seismic response. Because of the variable nature of the ground properties, other proxies such as geology are not sufficient to relevantly assess the ground amplification.

2D/3D effects are also critical to be recognized because they may greatly increase the local hazard. However, these effects are present only at particular sites that need to be recognized. In Switzerland, these sites are parts of the deep sediment valleys of the Rhône, Rhine, and Aar rivers as well as smaller structures like small alpine valleys, alluvial fans, and pronounced lateral changes in the velocity structure. The previously studied case of the Rhône Valley (e.g., Roten *et al.*, 2006) is a particular case with strong 2D effects. The highlighted cases will now be studied in more detail with 2D/3D characterization. Indeed, except for some well-studied cases, little is known of the geometry and the elastic properties of sedimentary valleys. This study also again confirmed the relevancy of the study by Bard and Bouchon (1985). The critical shape ratio and velocity contrasts they propose are in accordance with the observations presented here.

The use of ESM amplification directly within the combined inversion procedure of 1D cases is planned for future work. The case of structures with 2D/3D effects can be identified with the comparison, but a different approach needs to be developed to invert for the 2D structure (Roten and Fäh, 2007). Within the spectral modeling process, the anelastic attenuation term is also obtained in terms of site-specific kappa (Edwards *et al.*, 2011) and could be used to derive the quality factors of the sediments. Relating the inverted anelastic term of kappa from spectral modeling to attenuation models is therefore a topic for future work.

Besides site effects, numerous sites presented in this study cover aspects of different scientific and societal interest. It is the basis for future work on earthquake hazard and risk, including source effects, nonlinear site response and liquefaction, and earthquake-triggered landslides.

Data and Resources

Data from the SED permanent network used in this article can be obtained from the Arclink server of SED (arclink.ethz.ch; last accessed June 2014) or alternatively from the European Integrated waveform Data Archive (EIDA) node of ETH Zurich (eida.ethz.ch; last accessed June 2014). Geographical data from the Swiss Federal Office for Topography (Swisstopo) are used in this article. The data were partly processed using the Geopsy software suite (www.geopsy.org; last accessed December 2012) including geopsy and dinver. Some figures were made using the Quantum Geographic

Information System (QGIS) (http://qgis.osgeo.org/; last accessed September 2013).

Acknowledgments

The Renewal project of the Swiss Strong Motion Network (SSMNet) is supported by the Federal Office for the Environment (FOEN), the Federal Roads Office (FEDRO), Swiss Federal Nuclear Safety Inspectorate (ENSI), the Swiss Federal Railways (SBB), the Schweizerischer Pool für Erdbebendeckung, and ETH Zurich. The authors also thank Sabine Wöhlbier-Röthlisberger who produced Figure 1. They are also grateful to Associate Editor Stefano Parolai, Roberto Paolucci, and an anonymous reviewer for their help in the improvement of the article.

References

Aoi, S., T. Kunugi, and H. Fujiwara (2004). Strong-motion seismograph network operated by NIED: K-NET and KiK-net, *J. Jpn. Assoc. Earthq. Eng.* **4,** no. 3, 65–74, doi: 10.5610/jaee.4.3_65.

Bard, P.-Y., and M. Bouchon (1980). The seismic response of sediment-filled valleys. Part 2. The case of incident *P* and *SV* waves, *Bull. Seismol. Soc. Am.* **70,** no. 5, 1921–1941.

Bard, P.-Y., and M. Bouchon (1985). The two-dimensional resonance of sediment-filled valleys, *Bull. Seismol. Soc. Am.* **75,** no. 2, 519–541.

Bard, P.-Y., H. Cadet, B. Endrun, M. Hobiger, F. Renalier, N. Theodulidis, M. Ohrnberger, D. Fäh, F. Sabetta, P. Teves-Costa, *et al.* (2010). From non-invasive site characterization to site amplification: Recent advances in the use of ambient vibration measurements, in *Earthquake Engineering in Europe*, M. Garevski and A. Ansal (Editors), Vol. 17, Springer, Dordrecht, The Netherlands, 105–123, doi: 10.1007/978-90-481-9544-2.

Bard, P.-Y., M. Campillo, F. J. Chavez-Garcia, and F. Sanchez-Sesma (1988). The Mexico earthquake of September 19, 1985—A theoretical investigation of large- and small-scale amplification effects in the Mexico City Valley, *Earthq. Spectra* **4,** no. 3, 609–633, doi: 10.1193/1.1585493.

Bonnefoy-Claudet, S., F. Cotton, and P.-Y. Bard (2006). The nature of noise wavefield and its applications for site effects studies, *Earth-Science Rev.* **79,** nos. 3/4, 205–227, doi: 10.1016/j.earscirev.2006.07.004.

Building Seismic Safety Council (2004). *NEHRP Recommended Provisions for Seismic Regulations for New Buildings, and Other Structures (FEMA 450): Provisions*, National Institute of Building Sciences.

Burjánek, J., B. Edwards, and D. Fäh (2014). Empirical evidence of local seismic effects at sites with pronounced topography: A systematic approach, *Geophys. J. Int.* **197,** 608–619, doi: 10.1093/gji/ggu014.

Burjánek, J., G. Gassner-Stamm, V. Poggi, J. R. Moore, and D. Fäh (2010). Ambient vibration analysis of an unstable mountain slope, *Geophys. J. Int.* **180,** no. 2, 820–828, doi: 10.1111/j.1365-246X.2009.04451.x.

Burjánek, J., J. R. Moore, F. X. Yugsi Molina, and D. Fäh (2012). Instrumental evidence of normal mode rock slope vibration, *Geophys. J. Int.* **188,** no. 2, 559–569, doi: 10.1111/j.1365-246X.2011.05272.x.

Capon, J. (1969). High-resolution frequency-wavenumber spectrum analysis, *Proc. IEEE* **57,** no. 8, 1408–1418, doi: 10.1109/PROC.1969.7278.

Cauzzi, C., and J. Clinton (2013). A high- and low-noise model for high-quality strong-motion accelerometer stations, *Earthq. Spectra* **29,** no. 1, 85–102, doi: 10.1193/1.4000107.

Cauzzi, C., E. Faccioli, and G. Costa (2011). 1D and 2D site amplification effects at Tarcento (Friuli, NE Italy), 30 years later, *J. Seismol.* **15,** no. 1, 1–17, doi: 10.1007/s10950-010-9202-y.

Chavez-Garcia, F. J., W. R. Stephenson, and M. Rodríguez (1999). Lateral propagation effects observed at Parkway, New Zealand. A case history to compare 1D versus 2D site effects, *Bull. Seismol. Soc. Am.* **89,** no. 3, 718–732.

Clinton, J., C. Cauzzi, D. Fäh, C. Michel, P. Zweifel, M. Olivieri, G. Cua, F. Haslinger, and D. Giardini (2011). The current state of strong motion monitoring in Switzerland, in *Earthquake Data in Engineering Seismology*, S. Akkar, P. Gülkan, and T. van Eck (Editors), Vol. 14, Springer, Dordrecht, The Netherlands, 219–233, doi: 10.1007/978-94-007-0152-6.

Cornou, C., and P.-Y. Bard (2003). Site-to-bedrock over 1D transfer function ratio: An indicator of the proportion of edge-generated surface waves? *Geophys. Res. Lett.* **30,** no. 9, 1453, doi: 10.1029/2002GL016593.

Cornou, C., M. Ohrnberger, D. M. Boore, K. Kudo, and P.-Y. Bard (2009). Derivation of structural models from ambient vibration array recordings: Results from an international blind test, in *Third International Symposium on the Effects of Surface Geology on Seismic Motion*, Grenoble, France, 30 August–1 September 2006, 1127–1219.

Di Capua, G., G. Lanzo, V. Pessina, S. Peppoloni, and G. Scasserra (2011). The recording stations of the Italian strong motion network: Geological information and site classification, *Bull. Earthq. Eng.* **9,** no. 6, 1779–1796, doi: 10.1007/s10518-011-9326-7.

Ditommaso, R., M. Mucciarelli, M. R. Gallipoli, and F. Ponzo (2010). Effect of a single vibrating building on free-field ground motion: Numerical and experimental evidences, *Bull. Earthq. Eng.* **8,** no. 3, 693–703, doi: 10.1007/s10518-009-9134-5.

Duval, A.-M., S. Vidal, J.-P. Méneroud, A. Singer, F. De Santis, C. Ramos, G. Romero, R. Rodriguez, A. Pernia, N. Reyes, *et al.* (2001). Caracas, Venezuela, site effect determination with microtremors, *Pure Appl. Geophys.* **158,** no. 12, 2513–2523, doi: 10.1007/PL00001183.

Edwards, B., and D. Fäh (2013). A stochastic ground-motion model for Switzerland, *Bull. Seismol. Soc. Am.* **103,** no. 1, 78–98, doi: 10.1785/0120110331.

Edwards, B., D. Fäh, and D. Giardini (2011). Attenuation of seismic shear wave energy in Switzerland, *Geophys. J. Int.* **185,** no. 2, 967–984, doi: 10.1111/j.1365-246X.2011.04987.x.

Edwards, B., C. Michel, V. Poggi, and D. Fäh (2013). Determination of site amplification from regional seismicity: Application to the Swiss National Seismic Networks, *Seismol. Res. Lett.* **84,** no. 4, 611–621, doi: 10.1785/0220120176.

Edwards, B., A. Rietbrock, J. J. Bommer, and B. Baptie (2008). The acquisition of source, path, and site effects from microearthquake recordings using Q tomography: Application to the United Kingdom, *Bull. Seismol. Soc. Am.* **98,** no. 4, 1915–1935, doi: 10.1785/0120070127.

Ermert, L., V. Poggi, J. Burjánek, and D. Fäh (2014). Fundamental and higher 2-D resonance modes of an Alpine valley, *Geophys. J. Int.* **198,** no. 2, 795–811, doi: 10.1093/gji/ggu072.

Eurocode 8 (2004). Design of structures for earthquake resistance—Part 1: General rules, seismic actions and rules for buildings, EN 1998-1, European Committee for Standardization (CEN), Brussels, 1–229.

Faccioli, E., M. Villani, M. Vanini, and C. Cauzzi (2010). Mapping seismic hazard for the needs of displacement-based design, in *The Case of Italy, in Geotechnical, Geological and Earthquake Engineering–Advances in Performance-Based Earthquake Engineering*, M. N. Fardis (Editor), Vol. 13, Springer, Dordrecht, The Netherlands, 3–14, doi: 10.1007/978-90-481-8746-1_1.

Fäh, D., S. Fritsche, V. Poggi, G. Gassner-Stamm, P. Kästli, J. Burjánek, P. Zweifel, S. Barman, J. Clinton, L. Keller, P. Renault, and S. Heuberger (2009). *Determination of Site Information for Seismic Stations in Switzerland*, SED report SED/PRP/R/004/20090831, Zurich, Switzerland.

Fäh, D., F. Kind, and D. Giardini (2001). A theoretical investigation of average H/V ratios, *Geophys. J. Int.* **145,** 535–549.

Fäh, D., J. R. Moore, J. Burjánek, I. Iosifescu, L. A. Dalguer, F. Dupray, C. Michel, J. Woessner, A. Villiger, J. Laue, *et al.* (2012). Coupled seismogenic geohazards in Alpine region, *Bolletino Di Geofisica Teorica Ed Applicata* **53,** 485–508, doi: 10.4430/bgta0048.

Fäh, D., G. Stamm, and H.-B. Havenith (2008). Analysis of three-component ambient vibration array measurements, *Geophys. J. Int.* **172,** no. 1, 199–213, doi: 10.1111/j.1365-246X.2007.03625.x.

Field, E. H. (1996). Spectral amplification in a sediment-filled valley exhibiting clear basin-edge-induced waves, *Bull. Seismol. Soc. Am.* **86,** no. 4, 991–1005.

Foti, S., S. Parolai, P. Bergamo, G. Di Giulio, M. Maraschini, G. Milana, M. Picozzi, and R. Puglia (2011). Surface wave surveys for seismic site characterization of accelerometric stations in ITACA, *Bull. Earthq. Eng.* **9,** no. 6, 1797–1820, doi: 10.1007/s10518-011-9306-y.

Fritsche, S., D. Fäh, and D. Giardini (2005). Damage fields and site-effects. Investigations on the 1855 earthquake in Switzerland, in *250th Anniversary of the 1755 Lisbon Earthquake International Conference*, Lisbon, Portugal, 1–4 November 2005.

Gorini, A., M. Nicoletti, P. Marsan, R. Bianconi, R. Nardis, L. Filippi, S. Marcucci, F. Palmo, and E. Zambonelli (2010). The Italian strong motion network, *Bull. Earthq. Eng.* **8,** no. 5, 1075–1090, doi: 10.1007/s10518-009-9141-6.

Guéguen, P., C. Cornou, S. Garambois, and J. Banton (2007). On the limitation of the H/V spectral ratio using seismic noise as an exploration tool: Application to the Grenoble Valley (France), a small apex ratio basin, *Pure Appl. Geophys.* **164,** no. 1, 115–134, doi: 10.1007/s00024-006-0151-x.

Havenith, H.-B., D. Fäh, U. Polom, and A. Roullé (2007). *S*-wave velocity measurements applied to the seismic microzonation of Basel, Upper Rhine Graben, *Geophys. J. Int.* **170,** no. 1, 346–358, doi: 10.1111/j.1365-246X.2007.03422.x.

Hobiger, M., C. Cornou, M. Wathelet, G. Di Giulio, B. Knapmeyer-Endrun, F. Renalier, P.-Y. Bard, A. Savvaidis, S. Hailemikael, B. N. Le, M. Ohrnberger, and N. Theodoulidis (2012). Ground structure imaging by inversions of Rayleigh wave ellipticity: Sensitivity analysis and application to European strong-motion sites, *Geophys. J. Int.* **192,** no. 1, 207–229, doi: 10.1093/gji/ggs005.

Joyner, W. B. (2000). Strong motion from surface waves in deep sedimentary basins, *Bull. Seismol. Soc. Am.* **90,** no. 6B, S95–S112.

Joyner, W. B., R. E. Warrick, and T. E. Fumal (1981). The effect of Quaternary alluvium on strong ground motion in the Coyote Lake, California, earthquake of 1979, *Bull. Seismol. Soc. Am.* **71,** no. 4, 1333–1349.

Kawase, H. (1996). The cause of the damage belt in Kobe: "The Basin-Edge Effect," Constructive interference of the direct *S*-wave with the basin-induced diffracted/Rayleigh waves, *Seismol. Res. Lett.* **67,** no. 5, 25–34, doi: 10.1785/gssrl.67.5.25.

King, J. L., and B. E. Tucker (1984). Observed variations of earthquake motion across a sediment-filled valley, *Bull. Seismol. Soc. Am.* **74,** no. 1, 137–151.

Knopoff, L. (1964). A matrix method for elastic wave problems, *Bull. Seismol. Soc. Am.* **54,** no. 1, 431–438.

Le Roux, O., C. Cornou, D. Jongmans, and S. Schwartz (2012). 1-D and 2-D resonances in an Alpine valley identified from ambient noise measurements and 3-D modelling, *Geophys. J. Int.* **191,** no. 2, 579–590, doi: 10.1111/j.1365-246X.2012.05635.x.

Lebrun, B., D. Hatzfeld, and P.-Y. Bard (2001). Site effect study in urban area: Experimental results in Grenoble (France), *Pure Appl. Geophys.* **158,** no. 12, 2543–2557, doi: 10.1007/PL00001185.

Lee, C., C. Cheng, C. Liao, and Y. Tsai (2001). Site classification of Taiwan free-field strong-motion stations, *Bull. Seismol. Soc. Am.* **91,** no. 5, 1283–1297.

Lenti, L., S. Martino, A. Paciello, and G. Scarascia Mugnozza (2009). Evidence of two-dimensional amplification effects in an Alluvial Valley (Valnerina, Italy) from velocimetric records and numerical models, *Bull. Seismol. Soc. Am.* **99,** no. 3, 1612–1635, doi: 10.1785/0120080219.

Luzi, L., S. Lovati, E. D'Alema, S. Marzorati, D. Giacomo, S. Hailemikael, E. Cardarelli, M. Cercato, G. Di Filippo, G. Milana, *et al.* (2010). Italian accelerometric archive: Geological, geophysical and geotechnical investigations at strong-motion stations, *Bull. Earthq. Eng.* **8,** no. 5, 1189–1207, doi: 10.1007/s10518-009-9153-2.

McNamara, D. E., and R. P. Buland (2004). Ambient noise levels in the Continental United States, *Bull. Seismol. Soc. Am.* **94,** no. 4, 1517–1527, doi: 10.1785/012003001.

McNamara, D. E., C. R. Hutt, L. S. Gee, H. M. Benz, and R. P. Buland (2009). A method to establish seismic noise baselines for automated station assessment, *Seismol. Res. Lett.* **80,** no. 4, 628–637.

Odum, J. K., W. R. Stephenson, R. A. Williams, and C. von Hillebrandt-Andrade (2013). V_{S30} and spectral response from collocated shallow, active-, and passive-source V_S data at 27 sites in Puerto Rico, *Bull. Seismol. Soc. Am.* **103,** no. 5, 2709–2728, doi: 10.1785/0120120349.

Paolucci, R., and L. Morstabilini (2006). Non-dimensional site amplification functions for basin edge effects on seismic ground motion, in *Third International Symposium on the Effects of Surface Geology on Seismic Motion*, Grenoble, France, 30 August–1 September 2006, 823–831.

Park, C. B., R. D. Miller, and J. Xia (1999). Multichannel analysis of surface waves, *Geophysics* **64,** no. 3, 800–808, doi: 10.1190/1.1444590.

Poggi, V., and D. Fäh (2010). Estimating Rayleigh wave particle motion from three-component array analysis of ambient vibrations, *Geophys. J. Int.* **180,** no. 1, 251–267, doi: 10.1111/j.1365-246X.2009.04402.x.

Poggi, V., B. Edwards, and D. Fäh (2011). Derivation of a reference shear-wave velocity model from empirical site amplification, *Bull. Seismol. Soc. Am.* **101,** no. 1, 258–274, doi: 10.1785/0120100060.

Poggi, V., B. Edwards, and D. Fäh (2012). Characterizing the vertical to horizontal ratio of ground-motion at soft sediment sites, *Bull. Seismol. Soc. Am.* **102,** no. 6, 2741–2756.

Poggi, V., L. Ermert, J. Burjánek, C. Michel, and D. Fäh (2014). Modal analysis of 2-D sedimentary basin from frequency domain decomposition of ambient vibration array recordings, *Geophys. J. Int.* (in press).

Poggi, V., D. Fäh, J. Burjánek, and D. Giardini (2012). The use of Rayleigh-wave ellipticity for site-specific hazard assessment and microzonation: Application to the city of Lucerne, Switzerland, *Geophys. J. Int.* **188,** no. 3, 1154–1172, doi: 10.1111/j.1365-246X.2011.05305.x.

Poggi, V., D. Fäh, and D. Giardini (2013). Time–frequency–wavenumber analysis of surface waves using the continuous wavelet transform, *Pure Appl. Geophys.* **170,** no. 3, 319–335, doi: 10.1007/s00024-012-0505-5.

Poovarodom, N., and N. Plalinyot (2013). Site characterization in the Greater Bangkok area by microtremor observations, *J. Earthq. Eng.* **17,** no. 2, 209–226, doi: 10.1080/13632469.2012.707346.

Roten, D., and D. Fäh (2007). A combined inversion of Rayleigh wave dispersion and 2-D resonance frequencies, *Geophys. J. Int.* **168,** no. 3, 1261–1275, doi: 10.1111/j.1365-246X.2006.03260.x.

Roten, D., D. Fäh, C. Cornou, and D. Giardini (2006). Two-dimensional resonances in Alpine valleys identified from ambient vibration wavefields, *Geophys. J. Int.* **165,** no. 3, 889–905, doi: 10.1111/j.1365-246X.2006.02935.x.

Roten, D., D. Fäh, K. B. Olsen, and D. Giardini (2008). A comparison of observed and simulated site response in the Rhône valley, *Geophys. J. Int.* **173,** no. 3, 958–978, doi: 10.1111/j.1365-246X.2008.03774.x.

Sandıkkaya, M. A., M. T. Yılmaz, B. S. Bakır, and Ö. Yılmaz (2009). Site classification of Turkish national strong-motion stations, *J. Seismol.* **14,** no. 3, 543–563, doi: 10.1007/s10950-009-9182-y.

Savvaidis, A., H. Cadet, P. Guéguen, A. Panou, C. Michel, N. Theodulidis, and I. Kalogeras (2006). Accelerograph stations site characterization using ambient noise: Selected stations in Greece, in *Third International Symposium on the Effects of Surface Geology on Seismic Motion*, Grenoble, France, 30 August–1 September 2006, 791–800.

Steimen, S., D. Fäh, F. Kind, C. Schmid, and D. Giardini (2003). Identifying 2D resonance in microtremor wave fields, *Bull. Seismol. Soc. Am.* **93,** no. 2, 583–599.

Thompson, E. M., L. G. Baise, R. E. Kayen, and B. B. Guzina (2009). Impediments to predicting site response: Seismic property estimation and modeling simplifications, *Bull. Seismol. Soc. Am.* **99,** no. 5, 2927–2949, doi: 10.1785/0120080224.

Thompson, E. M., L. G. Baise, Y. Tanaka, and R. E. Kayen (2012). A taxonomy of site response complexity, *Soil Dyn. Earthq. Eng.* **41,** 32–43, doi: 10.1016/j.soildyn.2012.04.005.

Wald, D. J., and R. W. Graves (1998). The seismic response of the Los Angeles basin, California, *Bull. Seismol. Soc. Am.* **88,** no. 2, 337–356.

Wathelet, M. (2008). An improved neighborhood algorithm: Parameter conditions and dynamic scaling, *Geophys. Res. Lett.* **35,** no. 9, 1–5, doi: 10.1029/2008GL033256.

Wathelet, M., D. Jongmans, M. Ohrnberger, and S. Bonnefoy-Claudet (2008). Array performances for ambient vibrations on a shallow structure and consequences over V_S inversion, *J. Seismol.* **12,** no. 1, 1–19, doi: 10.1007/s10950-007-9067-x.

Yamanaka, H., K. Seo, and T. Samano (1989). Effects of sedimentary layers on surface-wave propagation, *Bull. Seismol. Soc. Am.* **79,** no. 3, 631–644.

Yong, A., A. Martin, K. Stokoe, and J. Diehl (2013). ARRA-funded VS30 measurements using multi-technique approach at strong-motion stations in California and Central-Eastern United States. Reston, Virginia, *U.S. Geol. Surv. Open-File Rept. 2013-1102*, 59.

Zaré, M., P.-Y. Bard, and M. Ghafory-Ashtiany (1999). Site characterizations for the Iranian strong motion network, *Soil Dyn. Earthq. Eng.* **18,** 101–123.

ETHZ-SED
Sonneggstrasse 5
CH-8092 Zurich, Switzerland
(C.M., B.E., V.P., J.B., C.C., D.F.)

University of California, San Diego
San Diego Supercomputer Center
MC 0505, 9500 Gilman Drive
La Jolla, California 92093-0505
(D.R.)

Manuscript received 7 April 2014;
Published Online 11 November 2014